Cellulose (2019) 26:7237–7251
https://doi.org/10.1007/s10570-019-02613-8

ORIGINAL RESEARCH

Preparation and evaluation of oxygen scavenging nanocomposite films incorporating cellulose nanocrystals and Pd nanoparticles in poly(ethylene-co-vinyl alcohol)

Adriane Cherpinski · Atanu Biswas · Jose M. Lagaron · Alain Dufresne · Sanghoon Kim · Megan Buttrum · Eduardo Espinosa · H. N. Cheng

Received: 26 March 2019 / Accepted: 1 July 2019 / Published online: 5 July 2019

Abstract There is current interest in active packaging, where the packaging material exhibits desirable functions in addition to containment of product. One of these functions is to reduce the oxygen content in the package in order to minimize product oxidation and spoilage, and prolong product shelf-life. In this work, we have developed novel nanocomposites, comprising cellulose nanocrystals and Pd nanoparticles embedded in an ethylene–vinyl alcohol copolymer (EVOH). The nanocellulose is a critical component in the nanocomposite because it acts not only as reducing agent for $PdCl_2$ but also as support for the dispersion of Pd nanoparticles on EVOH film and enhances the physical properties of the EVOH. Pd nanoparticles react with oxygen to serve as oxygen scavenger. The cellulose nanocrystals have also been optionally oxidized, and the increased presence of carboxyl groups favored a better distribution of the Pd nanoparticles, thereby enabling improved oxygen absorption. These features make the nanocomposites

A. Cherpinski · J. M. Lagaron
Novel Materials and Nanotechnology Group, IATA, CSIC, Av. Agustín Escardino 7, 46980 Paterna, Valencia, Spain

A. Biswas (✉) · S. Kim · M. Buttrum
U.S. Department of Agriculture, Agricultural Research Service, National Center for Agricultural Utilization Research, 1815 N. University St, Peoria, IL 61604, USA
e-mail: atanu.biswas@usda.gov

A. Dufresne
Université Grenoble Alpes, CNRS, Grenoble INP (Institute of Engineering Université Grenoble Alpes), LGP2, 38000 Grenoble, France

E. Espinosa
Chemical Engineering Department, Universidad de Córdoba, Campus of Rabanales, 14014 Córdoba, Spain

H. N. Cheng (✉)
U.S. Department of Agriculture, Agricultural Research Service, Southern Regional Research Center, 1100 Robert E. Lee Blvd, New Orleans, LA 70124, USA
e-mail: hn.cheng@usda.gov

promising candidates as active packaging materials. Included in this work are the preparation and the characterization of these materials.

Keywords Active packaging · Cellulose nanocrystals · Ethylene–vinyl alcohol copolymer · Polymer films · Nanocomposite · Oxygen scavenging · Palladium nanoparticles

Introduction

A current trend in polymer research is active packaging, which aims to impart active functionalities to packaging beyond simple containment or protection of the product. Active packaging has the capability of maintaining product quality, extending the product shelf life (thereby minimizing price reductions), and enhancing cost-effectiveness of the product (Damaj et al. 2015). One of the common features of active packaging is to control the atmosphere inside the packaging, such as oxygen and moisture (Arvanitoyannis 2012; Wilson 2007).

Additionally, consumer acceptance of advanced food packaging techniques has increased as a result of the improvement in the quality of the product (such as color, flavor and freshness). Reduction of oxygen and moisture can decrease the possibility of product oxidation, spoilage, and corrosion; different methods are being used, including antioxidants, oxygen absorbers, desiccants, and corrosion inhibitors (Farber et al. 2003). Amongst active packaging techniques, oxygen scavenging films have been recently developed.

Currently available oxygen scavengers are often inserted in the package in the form of a sachet. A problem of an oxygen scavenging film is the tendency of oxygen scavengers in the film to agglomerate, which can reduce not only the mechanical and thermal properties but also the oxygen absorbing capacity (Shin et al. 2011). A technical challenge is to design oxygen scavenging multilayer films without any agglomeration of the active ingredients.

Nanotechnology is a promising tool for active packaging because the nanomaterials have high surface-to-volume ratio and can enhance the functions of active substances utilized in the packaging. However, a polar polymer or surfactant is needed preferably to minimize aggregation of the nanoparticles in order to mitigate the high surface energy of nanoparticles (Dainelli et al. 2008; Kundu 2013; Mayer and Antonietti 1998).

Another recent development is the increasing use of agro-based materials and their derivatives as possible replacements for the synthetic polymers (Cheng et al. 2018). Such materials have the advantage of being easily available, cost competitive, nontoxic, eco-friendly and biodegradable. Some of the earlier attempts have involved the blends of synthetic polymers with biodegradable or biobased polymers (Masmoudi et al. 2016). Additional approaches have been developed involving entirely biobased materials and their derivatives (e.g., Biswas et al. 2018). Current trends suggest that biobased or biodegradable materials will be increasingly adopted in response to public awareness of plastic wastes and societal and legislative pressure.

As a nanomaterial and a biobased substance, nanocellulose has often been formulated into packaging films, particularly for food-related applications, and many review articles have appeared (Arora and Padua 2010; Wróblewska-Krepsztul et al. 2018). Cellulose nanocrystals (CNCs) are often obtained from wood pulp or cellulose fibers by an acid hydrolysis, giving rise to highly crystalline and rigid nanoparticles (Cirtiu et al. 2011). Chemical modifications can be performed on the surface hydroxyl groups of CNCs, in order to impart hydrophilic or hydrophobic character to the nanoparticle surface that can enhance the compatibility between CNC and the continuous matrix and improve the properties of the resulting nanocomposite. Examples of chemical modifications on nanocellulose include oxidation, esterification, etherification, silylation, and polymer grafting (Chakrabarty and Teramoto 2018; Islam et al. 2018; Masmoudi et al. 2016).

In addition to nanocellulose, a number of metal-based nanoparticles (NPs) have been incorporated into biobased materials, e.g., starch, cellulose, and chitosan (Wu et al. 2016). The approach of producing a CNC-supported palladium NPs can obviate the need for chemical reductants and also improve the stability and catalytic activity of Pd NPs. Whereas the mechanism of nanocellulose-metal NP binding is still not fully understood, the combined CNC-Pd NP system has several advantages. Certainly, cellulose (and CNC) are available, biodegradable, and sustainable, and they

should be attractive materials for commercial development (Wu et al. 2013). The reaction of cellulose with 2,2,6,6-tetramethylpiperidine-1-oxyl (TEMPO) is well known to convert C6 hydroxyl on the anhydrous glucose unit of cellulose, which provide enhanced functionality and hydrophilicity for cellulose (Tang et al. 2017). Nanocellulose surface is hydrophilic due to the hydroxyl groups present. Because most of the conventional CNCs are produced via sulfuric acid digestion, some sulfate esters likely reside at the surface. When the surface is further oxidized with TEMPO, aldehydes and carboxyls are formed, and all these functionalities may serve to effectively stabilize metal centers via the formation of dative bonds (Kaushik and Moores 2016).

Among the most efficient methods, the combined organic–inorganic nanocomposite technique (i.e., polymers embedded with metal nanoparticles) proved to be highly effective (Carbone et al. 2016). A possible bugbear is the tendency of the nanoparticles to self-agglomerate. Thus, a useful preparative strategy in order to achieve improved dispersion in an aqueous medium or a polymer matrix is to minimize the attractive interactions between the nanoparticles by modifying the surface of the particles or the use of additives such as polymeric surfactants (Kango et al. 2013). The properties of the resulting nanocomposite depend on the specific features of the nanoparticles, including their particle size, aspect ratio, specific surface area, volume fraction, polymer-particle compatibility, and dispersibility (Müller et al. 2017).

Poly(ethylene-co-vinyl alcohol) (EVOH) is commercially available, biodegradable, and attractive as a polymeric matrix for the design of nanocomposite films because the OH groups in the polymer can enhance compatibility with the nanoparticles (Rosa et al. 2009). EVOH is often used as a barrier for oxygen, CO_2, or organic vapor in food and beverage packages. Despite the fact that it is a synthetic polymer, EVOH is recyclable in the polyolefin regrind using existing infrastructure (Gavara et al. 2017). As EVOH is hydrophilic, it is often fabricated as part of a multilayer film between water-resistance polymer layers (Mokwena and Tang 2012).

In this work, we have combined some of the techniques previously described in order to produce novel and workable films that can scavenge oxygen and have acceptable properties in active packaging. These materials were based on CNCs and Pd NPs embedded in EVOH. The CNCs were also optionally oxidized, which permitted improved oxygen absorption of the resultant film. The nanocomposite films were characterized with various analytical techniques and their effectiveness in oxygen absorption was demonstrated.

Materials and methods

Materials

Ethylene–vinyl alcohol copolymer (containing 32 mol% of ethylene), sodium hydroxide (NaOH 97%), and poly(*N*,*N*-diallydimethylammonium chloride) (poly-DADMAC) were acquired from Sigma-Aldrich (St Louis, MO, USA). The following chemicals were purchased from Fisher Scientific (Pittsburgh, PA, USA): palladium chloride ($PdCl_2 > 95\%$), ethanol 100%, sodium hypochlorite (NaClO, 10–15% available), sodium bromide (NaBr 99%), hydrochloric acid (HCl 37.5%), TEMPO (2,2,6,6-tetramethylpiperidine 1-oxyl, 98%) and 2-propanol (99.9%). Dialysis membrane Spectra/Por® (MW cut-off = 3.5 kD) was purchased from Spectrum Chemical (New Brunswick, NJ, USA). Cellulose nanocrystals (CNC aqueous slurry ~ 12% and CNC freeze dried ~ 98%) were purchased from the University of Maine (Orono, ME, USA). Millipore de-ionized water (Burlington, MA, USA) was used for all the experiments.

Methods

Preparation of TEMPO-oxidized CNC (TOCNC)

Oxidation experiments were carried out as previously reported (Isogai and Kato 1998; Lin et al. 2012; Montanari et al. 2005; Saito et al. 2007). The CNCs (1 g) were suspended in water (100 mL) containing TEMPO (TO, 0.016 g, 0.1 mmol) and sodium bromide (0.1 g, 1 mmol). A solution of NaOCl was added continuously with stirring at 500 rpm at room temperature in order to start the oxidation. The reaction was continued until the desired amount of NaClO (1.3–5.0 mmol NaClO per gram of cellulose) was dispensed. Throughout the process, 0.5 N NaOH was added to the reaction with a pH–stat in order to keep the pH at 10 until no NaOH consumption was

observed. After oxidation, the reaction was quenched by the ethanol addition (ca. 1 mL), and 0.5 N HCl was added to increase the pH to 7. The resulting suspension of oxidized CNC (TOCNC) was washed and centrifuged three times with water, dialyzed, and then freeze-dried to yield a powder product. In this work the CNCs both in slurry and in powder form were subjected to TEMPO-oxidation to obtain samples called TOCNC-SP and TOCNC-PP, respectively.

Preparation of nano-sized cellulose/palladium (CNCs/PdNP)

The CNCs (0.3, 0.6 and 1 wt%) were added to water (5 mL), and $PdCl_2$ (0.3, 0.6 and 1 wt%) was added to water (5 mL). The pH was adjusted to 1 with HCl (37.5%). A mixture of $PdCl_2$ aqueous solution and CNC suspension was prepared and stirred for 20 min at room temperature in a 10–20 mL Biotage vial, similar to the method previously reported (Wu et al. 2013). The mixture was then placed in the Biotage microwave reactor (Biotage Initiator Microwave Synthesis Systems, Biotage AB, Uppsala, Sweden), which was programmed for 1 min pre-stirring and 2-h heating at 120 °C. After the reaction mixture was cooled to room temperature for the next procedure, the solution turned from pale brown to pale yellow color.

Preparation of EVOH solution and EVOH/CNCs/PdNP

For the preparation of EVOH solution, the polymer (10 wt%) was dissolved in a solvent mixture containing 2-propanol/water (70:30 v/v) and stirred at 100 °C for 1 h. The EVOH solution was mixed with the previous CNC/Pd NP solutions and cooled for the next procedure.

Film-casting procedure

For film casting, the EVOH/CNC/PdNP solution was spread on a K 101 Control Coater apparatus (RK Print-Coat Instruments Ltd., Royston, UK) with a speed setting of 2. A closely wound meter bar kept the filmogenic solutions at a controlled thickness such that the dried film had a thickness of 10 ± 2 µm. After spreading, the films were dried under laminar air flow for 15 min at room temperature.

Characterization of CNCs

X-ray diffraction analysis (XRD)

X-ray diffraction analysis of the CNC powder samples, TOCNC-SP and TOCNC-PP, was carried out on a Bruker D8 Discover instrument (Karlsruhe, Germany). A monochromatic source CuKα1 was used over an angular range of 5–50° at a scan speed of 1.56°/min. The Crystallinity Index (CI) of each CNC was computed with the use of the Segal Method (Segal et al. 1959).

Optical transmittance

The optical transmittance of 0.1 wt% solution was determined in a quartz cuvette using a Lambda 25 UV-Spectrometer (Perkin Elmer, Branford, CT, USA) from 400–800 nm. As reference, a spectrum of distilled water was obtained.

Cationic demand

Each of the CNC samples (unmodified CNC, TOCNC-SP and TOCNC-PP), at 0.04 g dried weight, was diluted in 1 L distilled water and dispersed with a pulp disintegrator for 10 min at 3000 rpm. Then, 10 mL of the suspension was added with magnetic stirring to 25 mL of the cationic polymer, poly-DADMAC, for 5 min. The mixture was then centrifuged for 90 min at 4000 rpm in a Model 6 K unit (Sigma Laborzentrifugen GmbH, Osterode am Harz, Germany). Thereafter, 10 mL of the supernatant were taken to a polyelectrolyte titrator (Mütek PCD 03, Herrsching, Germany), and an anionic polymer (sodium polyethylene sulphate) was added until the reading gave 0 mV. The amount of the anionic polymer consumed allowed the cationic demand to be calculated, according to the methodology described by Espinosa et al. (2017).

Carboxyl content

The carboxyl content of CNCs was determined by conductometric titration following the methodology previously published by Besbes et al. (2011).

Characterization of films

Film thickness and conditioning

Before evaluation, all samples were equilibrated in desiccators containing dried silica gel at a constant temperature of 25 °C for 1 week. The thickness of the films was measured with a Mitutoyo digital micrometer S00014 (Kawasaki, Japan). Three measurements at random positions of the film were made. Each reported value consisted of the average and the standard deviation. The accuracy was ± 0.001 mm.

Scanning electron microscopy (SEM)

The morphology of the EVOH films were evaluated via both cross-sections and surfaces on a Hitachi scanning electron microscope, S-4800 (Tokyo, Japan). The film cross-section was prepared by cryo-fracture of the EVOH films using liquid nitrogen. Each film was attached to beveled holders with conductive double-sided adhesive tape. A thin coating of gold and palladium was sputtered onto the specimen under vacuum. The specimen was then observed on the SEM using an accelerating voltage of 5 kV.

Transmission electronic microscopy (TEM)

The Pd nanoparticles in the CNCs/PdNP solution were directly deposited onto clamping holders. The morphology and distribution of the Pd NPs were observed on a Jeol 1010 transmission electronic microscope (Hitachi, Tokyo, Japan) at an accelerating voltage of 80 kV.

Fourier transform infrared (FTIR) spectroscopy

FTIR spectra were acquired on the attenuated total reflection (ATR) accessory (Golden Gate of Specac, Ltd., Orpington, U.K.), which was coupled to a Bruker Tensor 37 FTIR instrument (Rheinstetten, Germany). A typical spectrum was collected in the 4000–600 cm^{-1} range by averaging 20 scans at a resolution of 4 cm^{-1}.

Differential scanning calorimetry (DSC)

Thermal properties of neat EVOH, EVOH/CNC/PdNP, and EVOH/TOCNC/PdNP films were evaluated by DSC using a Q2000 MDSC instrument (TA Instruments, New Castle, DE, USA) under nitrogen atmosphere. A small piece of each film (5 mm × 5 mm) was cut and weighed (∼ 1 mg) into a Tzero hermetic aluminum pan and sealed. The sample was equilibrated to 10 °C and then heated to 200 °C under nitrogen at a rate of 10 °C/min. The sample was then cooled at the same rate to 10 °C, and this heat-cool process was repeated. The equipment was calibrated with indium standard. Each sample was run in triplicate. Signal processing was achieved with the TA Instruments Universal Analysis 2000 software (version 4.5A).

Thermogravimetric analysis (TGA)

TGA was conducted on a Q500 TGA instrument (TA Instruments, New Castle, DE, USA). Typically, a square piece of film (about 10 mm × 10 mm) was cut and placed on a tared, open platinum TGA pan. The sample was heated from room temperature up to 800 °C under nitrogen at a rate of 10 °C/min. Along with weight loss data, the differential thermogravimetric weight loss (DTG, %/°C) was recorded as well. Each sample was run in triplicate.

Water vapor permeability (WVP)

The WVP value was determined gravimetrically according to the ASTM E96-95 method. A small sample of the film was placed at the top of a Payne permeability cup (Ø = 3.5 cm) from Elcometer Sprl (Hermalle-sous-Argenteau, Belgium) that contained 5 mL distilled water. One side of the film was exposed to 100% RH, but not in direct contact with water. The cup and the film were then sealed with silicon rings and placed in a desiccator containing dried silica at 24 °C and 47% RH. An identical setup with aluminum films served as a control sample to estimate water loss through the seal. The cups were weighed periodically over a 24-h period with ± 0.0001 g accuracy. The water vapor transmission rate (WVTR), which could be converted to WVP when corrected for permeant partial pressure, was determined from the steady-state permeation slope obtained from the regression analysis of weight loss data per unit area versus time, from which the weight loss was calculated as the total cell loss minus the loss through the seal. Measurements were performed in triplicate.

Measurement of oxygen scavenging activity

The same method as reported earlier (Cherpinski et al. 2018) was used for the oxygen scavenging experiment. This involved round-bottom flasks (Schlenk) from VidraFoc S.A. (Barcelona, Spain) with a PTFE stopcock and a headspace volume of 50 cm^3. The flasks contained a valve for gas flushing, and O_2-sensitive sensor spot (PSt3, detection limit 15 ppb, 0–100% oxygen) from PreSens (Regensburg, Germany) was glued onto the inner side of the flasks for the oxygen depletion measurements. The sample films of same thickness were cut (4 × 4 cm^2) and placed in the flasks. The flask was subsequently flushed for 30 s at 1 bar with a gas mixture containing 1 vol.% oxygen, 4 vol.% hydrogen, and 95 vol.% nitrogen, which was provided by Abelló Linde, S.A. (Barcelona, Spain). The oxygen concentration in the cell was monitored by a non-destructive measurement method using the OXY-4 mini (PreSens) multi-channel fiber optic oxygen meter for simultaneous read-out of up to 4 oxygen sensors, used with sensors based on a 2-mm optical fiber. Oxygen concentrations over time were measured by linking the light-emitting (600–660 nm) optical fibers to the flask's inner sensing spots. The sensor emitted a certain amount of luminescence depending on the oxygen concentration in the cell that was calibrated to yield the concentration by the equipment. All measurements were carried out at 23 °C and 100% RH.

Statistical analysis

The test data were evaluated through analysis of variance (ANOVA) using STATGRAPHICS Centurion XVI v 16.1.03 from StatPoint Technologies, Inc. (Warrenton, VA, USA). Fisher's least significant difference (LSD) was used at the 95% confidence level ($p < 0.05$). Mean values and standard deviations were also calculated.

Results and discussion

Cationic demand, carboxyl content and optical transmittance

The stability of CNC suspension depends on the fiber surface charge. In order to study the stability of the different samples used in this work, the cationic demand and the carboxyl content were analyzed (Table 1). The cationic demand increases when CNC is subjected to TEMPO oxidation due in part to the increase in the carboxyl groups by the selective oxidation of the C6 primary hydroxyl groups of cellulose. These carboxyl functionalities increase the anionic charge on the cellulose surface, thereby enhancing repulsion and decreasing agglomeration among the fibers. A reduction in aggregated fibers result in greater surface area and expose more surface hydroxy groups. The hydrophilicity of the fibers is also enhanced (Serra et al. 2017). Moreover, these carboxyl groups on cellulose can directly interact with metal ions, thus obviating the use of anchoring molecules (Martins et al. 2017).

The optical transmittance of the CNC suspensions is associated with the content of nanofibrillated material, being more transparent when the size of cellulose nanocrystals is smaller (Table 1, column 4). The oxidized CNC samples present lower transparency values due to the presence of aggregates that correspond presumably to a higher specific surface area and stronger hydrogen bonding between the nanocrystals (Meng et al. 2019).

X-ray diffraction (XRD) analysis

The XRD patterns for CNCs are shown in Fig. 1. The diffraction peaks of CNCs at 2θ = 15.0, 16.5, 22.3 and 34.4 are assigned to the $(1\bar{1}0)$, (110), (200) and (004) planes, respectively, which represent the crystalline structure of cellulose I (French 2014). Cellulose II presents diffraction peaks at 12.1 and 20.1° associated with the $(1\bar{1}0)$ and (110) planes (Fortunati et al. 2016). TOCNC-SP presents only cellulose I contribution; however, TOCNC-PP and CNC powder contain both cellulose I and cellulose II polymorphs. Cellulose II usually ensues from cellulose I by two distinct routes, i.e., mercerization (alkali treatment), and regeneration (solubilization and recrystallization) or acid hydrolysis of mercerized cellulose, but the detailed mechanism of this phenomenon for nanocellulose is still being studied (O'Sullivan 1997; Xing et al. 2018). All samples present a crystallinity index around 70% due to the removal of most parts of amorphous regions; however, 30% of CNC composition is still composed of residual amorphous cellulose.

Table 1 Characterization of unmodified CNC powder and TEMPO-oxidized powder samples, TOCNC-SP and TOCNC-PP

Sample	Cationic demand (μeq/g)	Carboxyl content (μmol COOH/g)	T_{800} (%)
CNC powder	448.44 ± 38.44	64.88 ± 40.59	97.22
TOCNC-SP	1,284.89 ± 9.19	482.05 ± 58.43	57.38
TOCNC-PP	1,314.30 ± 0	418.94 ± 37.88	40.97

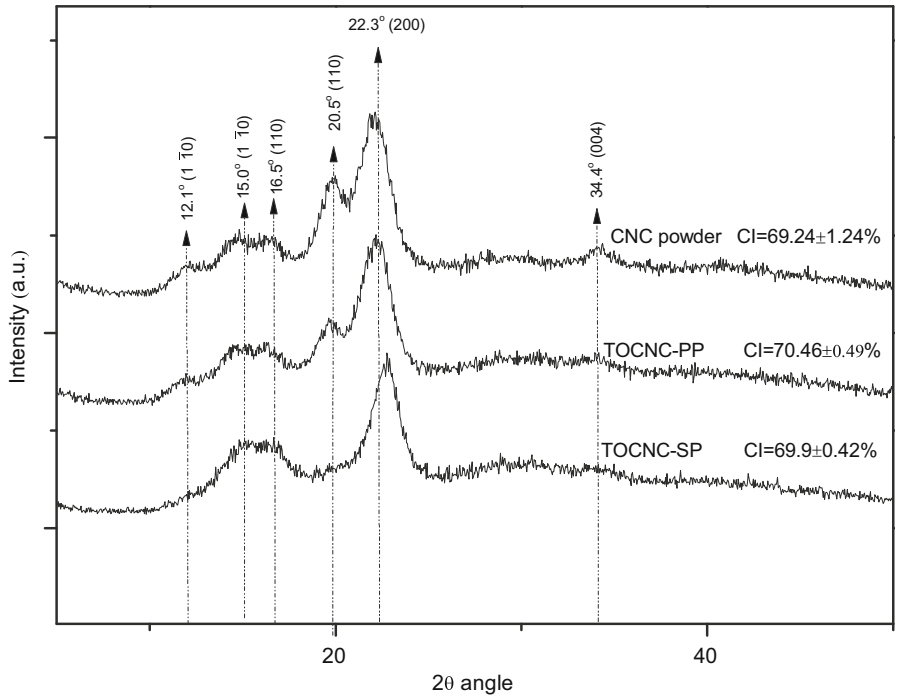

Fig. 1 XRD patterns of CNCs, the samples from top to bottom being unmodified CNC powder, TOCNC-PP, and TOCNC-SP

Morphology of nanocomposite Films

The contact transparency of neat EVOH film and EVOH with different concentrations of CNCs/Pd is shown in Fig. 2. All the films were found to exhibit similar contact transparency and significantly different from that of the neat EVOH film. Thus, a good dispersion of the PdNP must have been achieved. However, samples C, D and E with 0.6 and 1 wt% of PdNP showed a yellow color probably due to the presence of the Pd nanoparticles.

Scanning electron microscopy (SEM)

The morphology of the materials was analyzed by SEM. As observed in Fig. 3, the film surface (Fig. 3b, c) was altered by adding CNCs/PdNP and revealed roughness when compared with the neat EVOH film (Fig. 3a) that exhibited a relatively smoother surface.

Fig. 2 Photographs of films containing: **A** neat EVOH 10%; **B** EVOH/CNC (0.3% wt%)/PdNP (0.3 wt%); **C** EVOH/CNC (0.6 wt%)/PdNP (0.6 wt%); **D** EVOH/CNC (1 wt%)/PdNP (1 wt%); **E** EVOH/TOCNC (1 wt%)/PdNP (1 wt%)

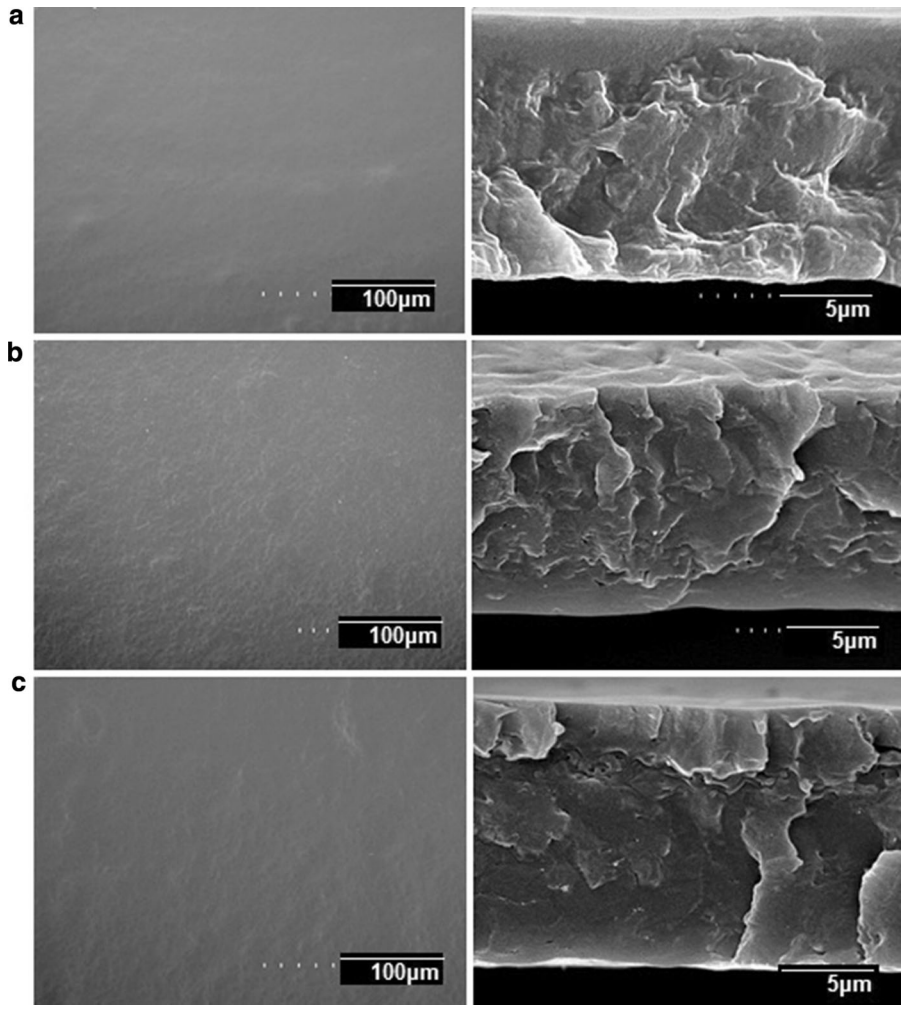

Fig. 3 Scanning electron microscopy (SEM) images taken on the surface view and cross-section: **a** EVOH film; **b** EVOH/CNC/PdNP film; **c** EVOH/TOCNC/PdNP film

The photomicrographs of the cross-sections obtained presented a similar morphology that verified the presence of spherical domains dispersed in a matrix for samples with CNCs/PdNP, without agglomerates, and this confirmed the efficient dispersion of the nanoparticles. This observation was in agreement with contact transparency data, which suggested that CNCs/PdNP particles were highly dispersed into the EVOH polymeric matrix.

Transmission electron microscopy (TEM)

Transmission electron microscopy was used to characterize the dispersion and the spatial distribution of PdNP onto CNC and TEMPO-treated CNC. Figure 4 shows a typical TEM image obtained for the dried CNCs/PdNP solutions, where some agglomeration of CNCs could be seen probably resulting from the drying process. The particle size of PdNP is important in the context of catalysis; in general, smaller particle sizes entail larger surface areas, which tend to enhance the catalytic process (Demir et al. 2004). In the present case, the diameter of PdNPs varied between 20 and 35 (± 5) nm and the CNCs acted as both the reducing agent and the support in the process. An analysis of the PdNP dispersion (Fig. 4a, b) clearly showed the observed difference. In Fig. 4a, the PdNPs were sparsely located on the CNC with partial aggregation; in comparison, the PdNPs supported by TOCNC (Fig. 4b) were homogeneously distributed on the

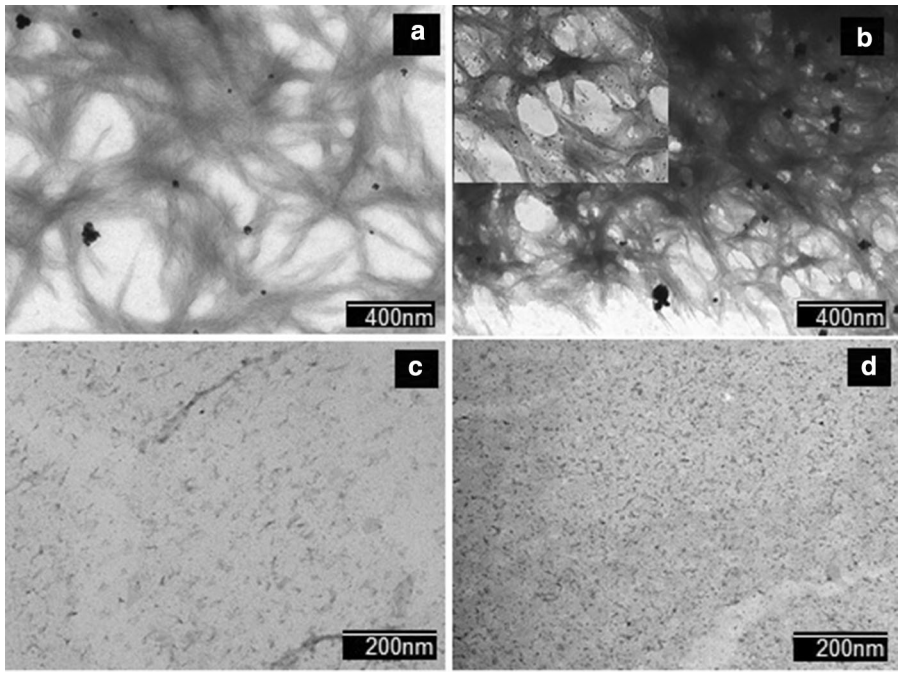

Fig. 4 Transmission electron microscopy (TEM) images taken directly from dried suspension of CNCs containing palladium nanoparticles (PdNPs): **a** CNC, **b** TOCNC; and TEM images taken from ultramicrotomed cross sections of the nanocomposite films: **c** EVOH/CNC/PdNP Film and **d** EVOH/TOCNC/PdNP Film

surface of CNC. This result confirmed the interaction between the PdNPs and the dissociated carboxyl groups on the surface of TOCNC, where the C atom of carboxyl group accepted the electrons from Pd, thereby enabling a more uniform immobilization of the PdNP on the TOCNC support (Chen et al. 2017). Figure 4c, d show TEM images taken on the nanocomposite films. From the images, CNC and PdNP can be observed to be intimately dispersed and distributed throughout the polymer matrix, being more evident in the TOCNC sample, as expected.

FTIR analysis of the EVOH films

FTIR studies were conducted to investigate the changes in chemical structure of TOCNC and respective EVOH films with CNCs/PdNP addition (Fig. 5). The IR spectrum for cellulose is well known, and some representative peaks can be found at 3200–3500 cm^{-1} (O–H stretching), 2850–3000 cm^{-1} (C–H stretching), and 1060–1162 cm^{-1} (C–O and C–O–C stretching bond); these peaks are not influenced by TO-mediated oxidation (Tang et al. 2017; Wu et al. 2013). When cellulose is selectively oxidized in position 6, the IR spectrum is known to change (da Silva Perez et al. 2003). The most important change in the spectrum of modified nanocellulose can be observed by the appearance of new bands at 1605 cm^{-1} and 1730 cm^{-1} that could be attributed to –COONa due to the C=O stretching of carboxyl groups and free carboxyl groups (Karim et al. 2017).

For EVOH film (Fig. 5) the characteristic peaks can be found at 3340 cm^{-1} (–OH stretching), 2945 cm^{-1} (–CH_2 anti-symmetric stretching) and 2912 cm^{-1} (–CH anti-symmetric stretching), 1417 cm^{-1} (–CH_2 asymmetric stretching) and 1336 cm^{-1} (–CH asymmetric stretching), 1092 cm^{-1} (C–O stretching), and 850 cm^{-1} (–CH out-of-plane deformation). Moreover, the peaks at 1650 and 850 cm^{-1} may possibly be associated with residual C=O or C=C group vibrations in EVOH (Wang et al. 2016). The 1% CNCs and 1% of PdNP added to the EVOH polymeric matrix were not enough to produce changes, as was shown by Choo et al. (2016), where they prepared poly(vinyl alcohol) (PVOH)-chitosan (CS) polymeric blends with different contents of TO-oxidized cellulose nanofiber (TOCN) (0, 0.5, 1.0 and 1.5 wt%) via the solution casting method. They observed only minor changes

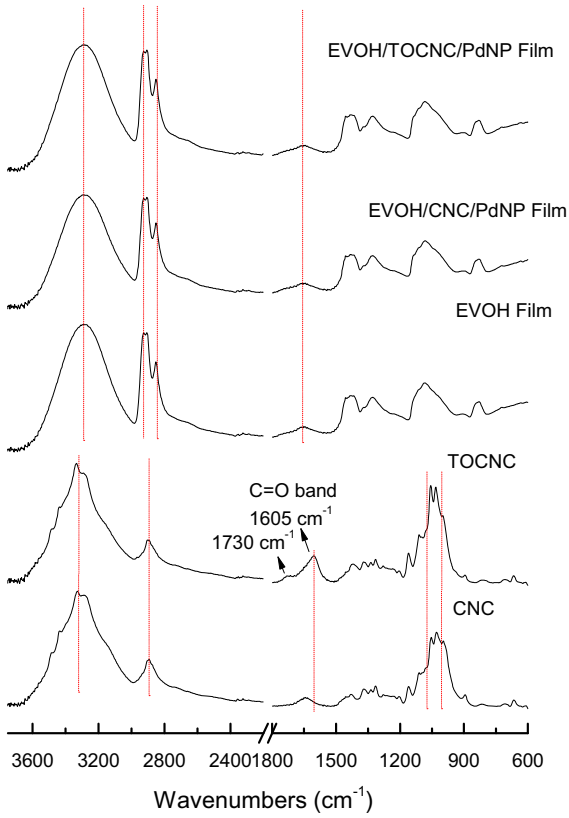

Fig. 5 ATR-FTIR spectra of the CNC, TOCNC, EVOH Film, EVOH/CNC/PdNP and EVOH/TOCNC/PdNP Films

due to the incorporation of TOCN that resulted from the low weight ratio of TOCN added to form the bio-nanocomposite films. Martínez-Sanz et al. (2013a) also observed that the characteristic bands from cellulose were only apparent for concentrations greater than 3 wt% bacterial CNCs in EVOH films.

Thermal analysis

For an investigation of how CNCs/PdNP content affected the thermal stability of EVOH nanocomposite films, DSC and TGA analyses were performed. Table 2 shows the glass transition temperature (T_g), melting temperature (T_m), and melting enthalpy (ΔH_m), and crystallization temperature (T_c) of the films as determined by DSC analysis of the dry samples. From the results, it can be seen that CNC reduces the polymer melting point, suggesting an antinucleating effect for the filler. This is confirmed by the observed reduction in crystallization temperature in the composites, which suggests that crystallization is hindered to some extent leading to smaller and more defective crystals. However, crystallinity was not observed to be reduced to a similar extent, suggesting that CNC does not impair crystallization but just leads to a more defective crystalline morphology, hence the lower melting point. The polymer T_g is also not affected to a significant extent by the presence of CNC.

The thermal stability of EVOH nanocomposite films evaluated by TGA is shown in Fig. 6 and Table 3. The EVOH nanocomposite films presented a two-step degradation pattern similar to that of neat EVOH; however, greater thermal resistance was observed for the EVOH nanocomposites, which indicated that the presence of CNCs/PdNP significantly influenced the thermal degradation patterns of the EVOH nanocomposite films.

In the TGA curves, an initial weight loss was observed for all samples, corresponding to the elimination of the absorbed moisture. Similar results were reported for EVA membranes by Puente et al. (2015), where the initial weight loss ($\sim$ 100 °C) was related to the water tightly bound to the polymer structure. In the DTG curves (Fig. 6d), a low temperature shoulder peak could be seen, which indicated the presence of some free water (Puente et al. 2015).

A decrease was observed in the maximum degradation rate for EVOH/TOCNC/PdNP film at 366 °C (Fig. 6d). The maximum degradation temperature for neat EVOH film was near 381 °C and for EVOH/CNC/PdNP film 394 °C, representing a decrease in the temperature of degradation about 15 and 28 °C, respectively. Fraschini et al. (2017) studied the thermal behavior of CNCs before and after oxidation, where an increase in the carboxyl content caused a gradual decrease in the thermal stability of the oxidized CNC samples. This was probably because the presence of charged groups on CNCs induced their earlier degradation during heating (Mariano et al. 2018). For all the samples, the residual weight of the nanocomposite films at 800 °C was consistent with the theoretical values.

An important observation was the onset decomposition temperature of EVOH/CNCs/PdNP nanocomposites, which was slightly higher than that of the neat EVOH film and EVOH/CNCs films (Fig. 6d), suggesting that the thermal stability of CNCs could be

Table 2 Thermal properties obtained by DSC in terms of glass transition (T_g), melting temperature (T_m), normalized melting enthalpy (ΔH_m), and crystallization temperature (T_c) for EVOH, EVOH/CNC/PdNP, and EVOH/TOCNC/PdNP films on first heating and subsequent crystallization runs

Sample	T_m (°C)	ΔH_m (J/g)	T_c (°C)	T_g (°C)
EVOH	166.6 ± 2.1	29.0 ± 3.0	160.2 ± 2.0	46.7 ± 0.8
EVOH/CNC PdNP	145.0 ± 1.4	29.8 ± 2.8	145.9 ± 3.8	45.2 ± 1.0
EVOH/TOCNC-PdNP	146.9 ± 1.1	26.6 ± 1.5	141.6 ± 3.5	45.3 ± 2.7

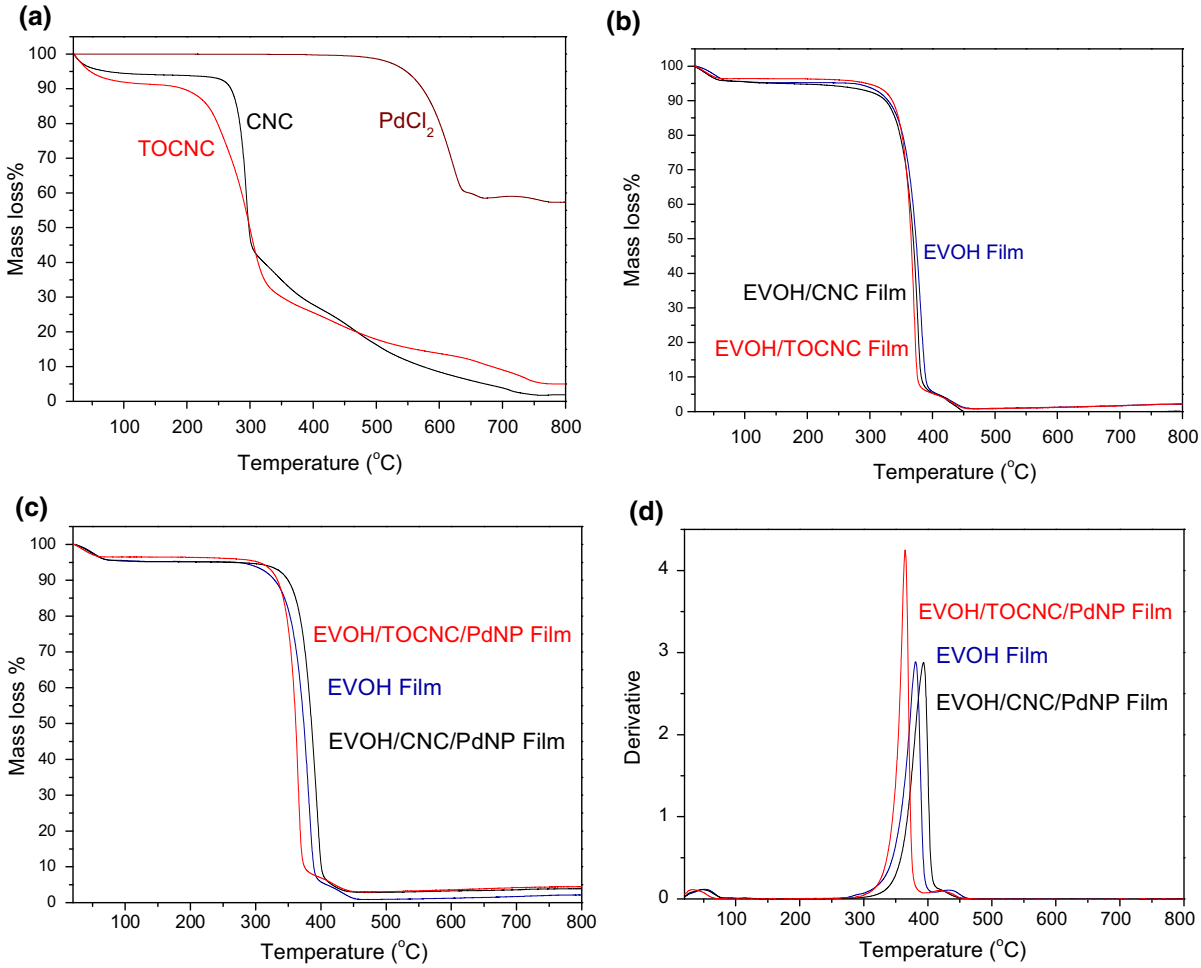

Fig. 6 Thermogravimetric analysis (TGA) curves for **a** CNC, TOCNC, $PdCl_2$, **b** EVOH/CNC, EVOH/TOCNC films and **c** EVOH film, EVOH/CNC/PdNP and EVOH/TOCNC/PdNP films, and **d** DTG curves for EVOH film, EVOH/CNC/PdNP and EVOH/TOCNC/PdNP films

improved by the incorporation of the palladium nanoparticles.

Water vapor permeability (WVP)

Table 4 shows the WVP value for the EVOH film and EVOH/CNCs/PdNP nanocomposites. The results indicated that EVOH films containing CNCs/PdNP

Table 3 Assessments of thermal stability obtained from thermogravimetric analysis (TGA) curves for CNC, TOCNC, EVOH/CNC, EVOH/TOCNC films, EVOH film EVOH/CNC/PdNP and EVOH/TOCNC/PdNP films, including degradation temperature at 5% of mass loss ($T_{5\ \%}$), maximum degradation temperature of the two degradation peaks (Td1, Td2), and residual mass at 800 °C (R800)

Film sample	$T_{5\ \%}$ (°C)	*T*d1 (°C)	*T*d2 (°C)	R_{800} (%)
CNC	219.3	298.8	–	–
TOCNC	158.7	312.2	–	–
EVOH/CNC film	256.2	387.0	458.9	1.9
EVOH/TOCNC film	285.3	377.4	457.6	2.1
EVOH Film	270.5	381.0	452.3	2.2
EVOH/CNC/PdNP film	285.1	394.3	445.1	3.9
EVOH/TOCNC/PdNP film	301.6	365.6	445.5	4.5

structures were not significantly different from neat EVOH film in terms of WVP values. Similar behavior was previously reported when bacterial cellulose CNCs incorporated into EVOH films showed a slight decrease in the water permeability of the nanocomposites, although the effect was not statistically significant for most of the samples (Martínez-Sanz et al. 2013b). However, Fortunati et al. (2013) obtained higher reduction in water permeability value (59%) for systems loaded with modified-CNCs (PLA/1s-CNC/1Ag and PLA/5s-CNC/1Ag), highlighting the beneficial effect of cellulose modification on the WVP barrier properties. The reason for the permeability observations here could be related to the distortion of the crystalline morphology anticipated by the above DSC results. Crystals are typically impermeable to the transport of low molecular weight compounds, and smaller and more defective crystals can result in reduced chain immobilization factor and hence increased amorphous density for the permeants to diffuse through (Lagarón 2011). The effects of CNC and PdNP in the nanocomplex, however, can be more complex.

Oxygen scavenging activity

Figure 7 shows the oxygen scavenging rate (OSR) for neat EVOH and EVOH CNCs/PDNP films. The oxygen absorption of the multilayer structures was studied at 23 °C, with an initial oxygen concentration of 1.0% in the headspace of the measuring flasks and 100% RH. The EVOH/TOCNC/PdNP film led to a faster and more significant decrease of O_2 rate. For EVOH/CNCs/PdNP (0.3/0.6 and 1%) films, the oxygen absorption (as expected) increased at nearly the same ratio as the oxygen scavenging content.

The TEM images (Fig. 4) suggested that the PdNPs were dispersed on the surface of CNC, but showed greater dispersion in the case of TOCNC for which the average particle size slightly decreased. For CNCs, PdNPs were also sparsely located with more nanoparticles agglomerated. For TOCNC, the abundant carboxylic acid groups made them available to interact with PdNP; thus, the EVOH film with TOCNC/PdNP showed faster oxygen activity compared with EVOH/CNC/PdNP film. In a previous work, a higher dispersion of the nanoparticles due to surfactant addition was shown to improve the O_2 depletion rate

Table 4 Water vapor permeability (WVP) for EVOH film, EVOH/CNC/PdNP film and EVOH/TOCNC/PdNP film

Sample	WVP $\times 10^{-14}$ (Kg m m^{-2} s^{-1} Pa^{-1})*
EVOH film	1.28 (2.3)[a]
EVOH/CNC/PdNP film	1.33 (3.3)[a]
EVOH/TOCNC/PdNP film	1.45 (2.6)[a]

*Mean value (standard error). The same superscript letter represents no statistically significant differences among the three samples ($p < 0.05$)

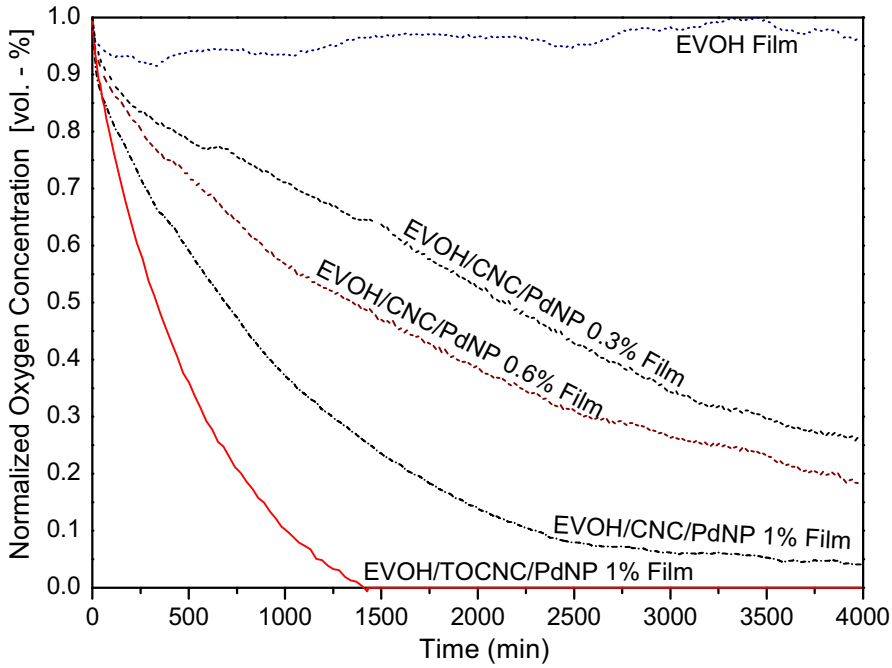

Fig. 7 Oxygen depletion for EVOH film without palladium nanoparticles (PdNPs), EVOH/CNC/PdNP (0.3, 0.6 and 1 wt%), EVOH/TOCNC/PdNP (1 wt%) films. Values were measured at 100% relative humidity (RH)

(Cherpinski et al. 2018). In a further study of the topic, the oxygen scavenging of the PdNPs was enhanced by incorporating them within polycaprolactone, a more oxygen permeable material (Cherpinski et al. 2019). The use of capping agents can reduce or prevent aggregation but also tends to decrease the reactivity of the surface, thereby decreasing the catalytic activity of the stabilized nanoparticles. Thus, CNC can be employed as an alternative to minimize aggregation without blocking access to the reactive surface atoms (Rezayat et al. 2014).

Another important aspect of OSR is the effect of humidity. Water molecules that are absorbed by EVOH at high RH levels are believed to interact with OH groups in the polymer matrix and weaken the hydrogen bonding among polymer molecules (Zhang et al. 2001). Because samples were exposed at 100% RH, the hydrophilic nature of the substrate materials presumably contribute to an accelerated water adsorption on the surface, which in turn might also promote the catalytic reaction of palladium (Yildirim et al. 2015).

Conclusions

In this work, several techniques were employed in order to produce a novel active packaging material that could scavenge oxygen effectively. CNC was a critical component in the nanocomposite because it acted not only as reducing agent for $PdCl_2$ but also as support for the deposition of PdNP on EVOH. PdNP absorbed oxygen and furnished the beneficial function of oxygen scavenging for the packaging film. EVOH was chosen as the polymer matrix because it is a water-soluble polymer that is often used as oxygen barrier in packaging. Oxidation of CNC with TEMPO improved oxygen absorption. The resulting nanocomposite films seem to have promising active packaging properties.

Acknowledgments Adriane Cherpinski would like to thank the Brazilian Council for Scientific and Technological Development (CNPq) of the Brazilian Government for supporting her stay at USDA Peoria laboratories. This study would not have been possible without the financial support of her predoctoral Grant (205955/2014-2). Eduardo Espinosa is grateful to the Spanish Ministry of Science and Education for support his research through the National Program FPU (Grant Number FPU14/02278). The authors would also like to acknowledge the funding by the MINECO project of the Spanish Government AGL2015-63855-C2-1-R. The authors acknowledge the expert technical assistance of Jason Adkins at USDA and helpful suggestions from Dr. A. D. French. Mention of trade names or commercial products in this publication is

solely for the purpose of providing specific information and does not imply recommendation or endorsement by the U.S. Department of Agriculture. USDA is an equal opportunity provider and employer.

References

Arora A, Padua G (2010) Nanocomposites in food packaging. J Food Sci 75(1):R43–R49

Arvanitoyannis I (2012) Modified atmosphere and active packaging technologies. CRC Press, Boca Raton

Besbes I, Alila S, Boufi S (2011) Nanofibrillated cellulose from TEMPO-oxidized eucalyptus fibres: effect of the carboxyl content. Carbohydr Polym 84(3):975–983

Biswas A, Furtado RF, Bastos MSR, Benevides SD, Oliveira MA, Boddu V, Cheng HN (2018) Preparation and characterization of carboxymethyl cellulose films with embedded essential oils. J Mater Sci Res 7:16–25

Carbone M, Donia DT, Sabbatella G, Antiochia R (2016) Silver nanoparticles in polymeric matrices for fresh food packaging. J King Saud Univ Sci 28(4):273–279

Chakrabarty A, Teramoto Y (2018) Recent advances in nanocellulose composites with polymers: a guide for choosing partners and how to incorporate them. Polymers 10(5):517

Chen Y, Chen S, Wang B, Yao J, Wang H (2017) TEMPO-oxidized bacterial cellulose nanofibers-supported gold nanoparticles with superior catalytic properties. Carbohydr Polym 160:34–42

Cheng HN, Gross RA, Smith PB (2018) Green polymer chemistry: new products, processes, and applications. In: (ACS symposium series, number 1310). American Chemical Society, Washington, DC

Cherpinski A, Gozutok M, Sasmazel H, Torres-Giner S, Lagaron JM (2018) Electrospun oxygen scavenging films of poly (3-hydroxybutyrate) containing palladium nanoparticles for active packaging applications. Nanomaterials 8(7):469

Cherpinski A, Szewczyk PK, Gruszczyński A, Stachewicz U, Lagaron JM (2019) Oxygen-scavenging multilayered biopapers containing palladium nanoparticles obtained by the electrospinning coating technique. Nanomaterials 9(2):262

Choo K, Ching YC, Chuah CH, Julai S, Liou NS (2016) Preparation and characterization of polyvinyl alcohol-chitosan composite films reinforced with cellulose nanofiber. Materials 9(8):644

Cirtiu CM, Dunlop-Briere AF, Moores A (2011) Cellulose nanocrystallites as an efficient support for nanoparticles of palladium: application for catalytic hydrogenation and Heck coupling under mild conditions. Green Chem 13(2):288–291

da Silva Perez D, Montanari S, Vignon MR (2003) TEMPO-mediated oxidation of cellulose III. Biomacromolecules 4(5):1417–1425

Dainelli D, Gontard N, Spyropoulos D, Zondervan-van den Beuken E, Tobback P (2008) Active and intelligent food packaging: legal aspects and safety concerns. Trends Food Sci Technol 19:S103–S112

Damaj Z, Joly C, Guillon E (2015) Toward new polymeric oxygen scavenging systems: formation of poly (vinyl alcohol) oxygen scavenger film. Packag Technol Sci 28(4):293–302

Demir MM, Gulgun MA, Menceloglu YZ, Erman B, Abramchuk SS, Makhaeva EE, Khokhov AR, Matveeva VG, Sulman MG (2004) Palladium nanoparticles by electrospinning from poly (acrylonitrile-co-acrylic acid)—$PdCl_2$ solutions. Relations between preparation conditions, particle size, and catalytic activity. Macromolecules 37(5):1787–1792

Espinosa E, Domínguez-Robles J, Sánchez R, Tarrés Q, Rodríguez A (2017) The effect of pre-treatment on the production of lignocellulosic nanofibers and their application as a reinforcing agent in paper. Cellulose 24(6):2605–2618

Farber JN, Harris LJ, Parish ME, Beuchat LR, Suslow TV, Gorney JR, Garrett EH, Busta FF (2003) Microbiological safety of controlled and modified atmosphere packaging of fresh and fresh-cut produce. Compr Rev Food Sci Food Saf 2:142–160

Fortunati E, Peltzer M, Armentano I, Jiménez A, Kenny JM (2013) Combined effects of cellulose nanocrystals and silver nanoparticles on the barrier and migration properties of PLA nano-biocomposites. J Food Eng 118(1):117–124

Fortunati E, Luzi F, Jiménez A, Gopakumar DA, Puglia D, Thomas S, Kenny JM, Chiralt A, Torre L (2016) Revalorization of sunflower stalks as novel sources of cellulose nanofibrils and nanocrystals and their effect on wheat gluten bionanocomposite properties. Carbohydr Polym 149:357–368

Fraschini C, Chauve G, Bouchard J (2017) TEMPO-mediated surface oxidation of cellulose nanocrystals (CNCs). Cellulose 24(7):2775–2790

French AD (2014) Idealized powder diffraction patterns for cellulose polymorphs. Cellulose 21(2):885–896

Gavara R, Catalá-Moragrega R, López-Carballo G, Cerisuelo JP, Domínguez I, Muriel-Galet V, Hernández-Muñoz P (2017) Use of EVOH for food packaging applications. Elsevier, Amsterdam. https://doi.org/10.1016/B978-0-08-100596-5.21125-6

Islam M, Chen L, Sisler J, Tam K (2018) Cellulose nanocrystal (CNC)–inorganic hybrid systems: synthesis, properties and applications. J Mater Chem B 6(6):864–883

Isogai A, Kato Y (1998) Preparation of polyuronic acid from cellulose by TEMPO-mediated oxidation. Cellulose 5(3):153–164

Kango S, Kalia S, Celli A, Njuguna J, Habibi Y, Kumar R (2013) Surface modification of inorganic nanoparticles for development of organic–inorganic nanocomposites—a review. Prog Polym Sci 38(8):1232–1261

Karim Z, Hakalahti M, Tammelin T, Mathew AP (2017) In situ TEMPO surface functionalization of nanocellulose membranes for enhanced adsorption of metal ions from aqueous medium. RSC Adv 7(9):5232–5241

Kaushik M, Moores A (2016) Nanocelluloses as versatile supports for metal nanoparticles and their applications in catalysis. Green Chem 18(3):622–637

Kundu S (2013) A new route for the formation of Au nanowires and application of shape-selective Au nanoparticles in SERS studies. J Mater Chem C 1(4):831–842

Lagarón JM (2011) Multifunctional and nanoreinforced polymers for food packaging. In: Lagaron JM (ed) Multifunctional and nanoreinforced polymers for food packaging. Elsevier/Woodhead Publishing, Oxford, pp 1–28

Lin N, Bruzzese CC, Dufresne A (2012) TEMPO-oxidized nanocellulose participating as crosslinking aid for alginate-based sponges. ACS Appl Mater Interf 4(9):4948–4959

Mariano M, El Kissi N, Dufresne A (2018) Cellulose nanomaterials: size and surface influence on the thermal and rheological behavior. Polímeros 28(2):93–102

Martínez-Sanz M, Lopez-Rubio A, Lagaron JM (2013a) Nanocomposites of ethylene vinyl alcohol copolymer with thermally resistant cellulose nanowhiskers by melt compounding (I): morphology and thermal properties. J Appl Polym Sci 128(5):2666–2678

Martínez-Sanz M, Lopez-Rubio A, Lagaron JM (2013b) Nanocomposites of ethylene vinyl alcohol copolymer with thermally resistant cellulose nanowhiskers by melt compounding (II): water barrier and mechanical properties. J Appl Polym Sci 128(3):2197–2207

Martins GB, Santos MRD, Rodrigues MV, Sucupira RR, Meneghetti L, Monteiro AL, Suarez PA (2017) Cellulose oxidation and the use of carboxyl cellulose metal complexes in heterogeneous catalytic systems to promote Suzuki-Miyaura coupling and CO bond formation reaction. J Braz Chem Soc 28(11):2064–2072

Masmoudi F, Bessadok A, Dammak M, Jaziri M, Ammar E (2016) Biodegradable packaging materials conception based on starch and polylactic acid (PLA) reinforced with cellulose. Environ Sci Pollut Res 23(20):20904–20914

Mayer A, Antonietti M (1998) Investigation of polymer-protected noble metal nanoparticles by transmission electron microscopy: control of particle morphology and shape. Coll Polym Sci 276(9):769–779

Meng F, Wang G, Du X, Wang Z, Xu S, Zhang Y (2019) Extraction and characterization of cellulose nanofibers and nanocrystals from liquefied banana pseudo-stem residue. Compos Part B Eng 160:341–347

Mokwena KK, Tang J (2012) Ethylene vinyl alcohol: a review of barrier properties for packaging shelf stable foods. Crit Rev Food Sci Nutr 52(7):640–650

Montanari S, Roumani M, Heux L, Vignon MR (2005) Topochemistry of carboxylated cellulose nanocrystals resulting from TEMPO-mediated oxidation. Macromolecules 38(5):1665–1671

Müller K, Bugnicourt E, Latorre M, Jorda M, Echegoyen-Sanz Y, Lagaron JM, Miesbauer O, Bianchin A, Hankin S, Bölz U, Pérez G, Jesdinszki M, Lindner M, Scheuerer Z, Castelló S, Schmid M (2017) Review on the processing and properties of polymer nanocomposites and nanocoatings and their applications in the packaging, automotive and solar energy fields. Nanomaterials 7(4):74

O'Sullivan AC (1997) Cellulose: the structure slowly unravels. Cellulose 4(3):173–207

Puente JAS, Fatyeyeva K, Marais S, Dargent E (2015) Multifunctional hydrolyzed EVA membranes with tunable microstructure and water barrier properties. J Membr Sci 480:93–103

Rezayat M, Blundell RK, Camp JE, Walsh DA, Thielemans W (2014) Green one-step synthesis of catalytically active palladium nanoparticles supported on cellulose nanocrystals. ACS Sustain Chem Eng 2(5):1241–1250

Rosa MF, Chiou BS, Medeiros ES, Wood DF, Mattoso LH, Orts WJ, Imam SH (2009) Biodegradable composites based on starch/EVOH/glycerol blends and coconut fibers. J Appl Polym Sci 111(2):612–618

Saito T, Kimura S, Nishiyama Y, Isogai A (2007) Cellulose nanofibers prepared by TEMPO-mediated oxidation of native cellulose. Biomacromolecules 8(8):2485–2491

Segal L, Creely J, Martin A Jr, Conrad C (1959) An empirical method for estimating the degree of crystallinity of native cellulose using the X-ray diffractometer. Text Res J 29(10):786–794

Serra A, González I, Oliver-Ortega H, Tarrès Q, Delgado-Aguilar M, Mutjé P (2017) Reducing the amount of catalyst in TEMPO-oxidized cellulose nanofibers: effect on properties and cost. Polymers 9(11):557

Shin Y, Shin J, Lee YS (2011) Preparation and characterization of multilayer film incorporating oxygen scavenger. Macromol Res 19(9):869

Tang Z, Li W, Lin X, Xiao H, Miao Q, Huang L, Chen L, Wu H (2017) TEMPO-oxidized cellulose with high degree of oxidation. Polymers 9(9):421

Wang H, Zhang H, Niu B, Jiang S, Cheng J, Jiang S (2016) Structure and properties of the poly (vinyl alcohol-co-ethylene)/montmorillonite-phosphorylated soybean protein isolate barrier film. RSC Adv 6(35):29294–29302

Wilson CL (2007) Intelligent and active packaging for fruits and vegetables. CRC Press, Boca Raton

Wróblewska-Krepsztul J, Rydzkowski T, Borowski G, Szczypiński M, Klepka T, Thakur VK (2018) Recent progress in biodegradable polymers and nanocomposite-based packaging materials for sustainable environment. Int J Polym Anal Charact 23(4):383–395

Wu X, Lu C, Zhang W, Yuan G, Xiong R, Zhang X (2013) A novel reagentless approach for synthesizing cellulose nanocrystal-supported palladium nanoparticles with enhanced catalytic performance. J Mater Chem A 1(30):8645–8652

Wu X, Shi Z, Fu S, Chen J, Berry RM, Tam KC (2016) Strategy for synthesizing porous cellulose nanocrystal supported metal nanocatalysts. ACS Sustain Chem Eng 4(11):5929–5935

Xing L, Gu J, Zhang W, Tu D, Hu C (2018) Cellulose I and II nanocrystals produced by sulfuric acid hydrolysis of Tetrapak cellulose I. Carbohydr Polym 192:184–192

Yildirim S, Röcker B, Rüegg N, Lohwasser W (2015) Development of palladium-based oxygen scavenger: optimization of substrate and palladium layer thickness. Packag Technol Sci 28(8):710–718

Zhang Z, Britt IJ, Tung MA (2001) Permeation of oxygen and water vapor through EVOH films as influenced by relative humidity. J Appl Polym Sci 82(8):1866–1872